Dalton Transactions

Accepted Manuscript

ROYAL SOCIETY OF CHEMISTRY

www.rsc.org/dalton

Journal Name

ARTICLE

Synthesis, Crystal Structure and Magnetic Properties of $H_2tppz[ReCl_6]$ and $[Cu(bpzm)_2(\mu\text{-}Cl)ReCl_3(\mu\text{-}ox)Cu(bpzm)_2(\mu\text{-}ox)ReCl_3(\mu\text{-}Cl)]_n$

Received 00th January 20xx,
Accepted 00th January 20xx

DOI: 10.1039/x0xx00000x

www.rsc.org/

I. Gryca[a], J. Palion-Gazda[a], B. Machura[a,*], M. Penkala[b], R. Kruszyński[c], J. Cano[d,e], F. Lloret[d] and M. Julve[d,*]

Two new Re(IV) compounds of formula $H_2tppz[ReCl_6]$ (**1**) and $[Cu(bpzm)_2(\mu\text{-}Cl)ReCl_3(\mu\text{-}ox)Cu(bpzm)_2(\mu\text{-}ox)ReCl_3(\mu\text{-}Cl)]_n$ (**2**) [*tppz* = 2,3,5,6-tetrakis(2-pyridyl)pyrazine and *bpzm* = bis(pyrazolyl-1-yl)methane] have been prepared and their crystal structures determined by X-ray diffraction on single crystals. The compound **1** is a mononuclear species whose structure consists of octahedral hexachlororhenate(IV) anions and diprotonated H_2tppz^{2+} cations which are arranged in the unit cell as alternating anionic and cationic layers, held together by electrostatic forces. The structure of **2** is made up of alternating $[Cu(1)(bpzm)_2]^{2+}$ and $[(ox)ReCl_3(\mu\text{-}Cl)Cu(2)(bpzm)_2(\mu\text{-}Cl)ReCl_3(ox)]^{2-}$ entities interlinked by oxalate bridges to afford a neutral heterobimetallic chain. The oxalate group adopts the didentate (at Re)/monodentate (at Cu) bridging mode. The magnetic behavior of **1** and **2** has been investigated over the temperature range 1.9-295 K. **1** is a magnetically diluted Re(IV) complex, the relatively large value of the zero-field splitting of the ground level (D = -15.8(2) cm^{-1}) accounting for the variation of $\chi_M T$ in the low temperature range. Weak intrachain ferromagnetic interactions between Re(IV) and Cu(II) through oxalate (J_1 = +0.15 cm^{-1}) and single chloro (J_2 = +4.9 cm^{-1}) bridges occurs in **2** which are obscured by the large zero-field splitting of the Re(IV) ion (D_{Re}= 42 cm^{-1}). In addition, interchain antiferromagnetic interactions are also involved in **2** which are responsible for the metamagnetic behavior observed, the value of the critical dc magnetic field (H_c) being 20 kOe.

Introduction

In recent years, an important amount of work has been devoted to study the magnetic properties of hexahalorhenate(IV) complexes of general formula $(Cat)_m[ReX_6]$ {*Cat* = p-toluidinium ion, Li^+, Na^+, K^+, Rb^+, Cs^+, NH_4^+, Ag^+, NBu_4^+, $AsPh_4^+$, $[N(CH_3)_4]^+$, $[N(C_2H_5)_4]^+$, $[Fe(C_5R_5)_2]^+$, $(MePPh_3)^+$, $(BEDT\text{-}TTF)^{2+}$, $(DM\text{-}BEDT\text{-}TTF)^{2+}$, $H_4cyclam^{4+}$,$(H_3O.18\text{-}crown\text{-}6)^+$, Hpy^+, Hqy^+, $(H\text{-}4,4'\text{-}dmbpy)^+$, H_4biim^{2+}, $(m\text{-}rad)^+$, $(p\text{-}rad)^+$, $[RuCl(NH_3)_5]^{2+}$ and $[RuCl_2(en)_2]^+$ with X = F^-, Cl^-, Br^- or I^-}[1-18] and heterometallic complexes containing Re(IV) and 3d transition metal ions M(II) bridged by oxygen-donor oxalate (ox) and malonate (mal) ligands as well as cyanido groups from the $[ReCl_4(ox)]^{2-}$/$[ReBr_4(ox)]^{2-}$,[19-34] $[ReCl_4(mal)]^{2-}$[35-37] and trans-$[ReCl_4(CN)_2]^{2-}$[38-45] precursor complexes, respectively. Six-coordinate rhenium(IV) ($5d^3$ ion, t_{2g}^3 electronic configuration, $^4A_{2g}$ ground term) has a large magnetic anisotropy arising from spin–orbit coupling associated with the third-row transition metal ion and also a larger diffuseness of its magnetic orbitals when compared to the more contracted 3d orbitals. These features affect the nature and magnitude of the interaction

[a] Department of Crystallography, Institute of Chemistry, University of Silesia, 9th Szkolna St., 40-006 Katowice, Poland. *E-mail: basia@ich.us.edu.pl.
[b] Department of Inorganic, Organometallic Chemistry and Catalysis, Institute of Chemistry, University of Silesia, 9th Szkolna St., 40-006 Katowice, Poland.
[c] Department of X-ray Crystallography and Crystal Chemistry, Institute of General and Ecological Chemistry, Lodz University of Technology,116 Żeromski St., 90-924 Łodź, Poland.
[d] Departament de Quimica Inoganica(Instituto de Ciencia Molecular (ICMol), Universitat de Valencia, C/ Catedratico Jose Beltran 2, 46980 Paterna (Valencia), Spain. *E-mail: miguel.julve@uv.es
[e] Fundacio General de la Universitat de Valencia (FGUV), Universitat de Valencia, 46010Valencia, Spain.

†Electronic Supplementary Information (ESI) available: XRPD [Figs. S1 (**1**) and S2 (**2**)], conformations of the H_2tppz^{2+} dication (Figs. S3 and S4), intermolecular interactions for **1** and **2** (Table S1), bond lengths and angles for **1** (Table S2), structural data for compounds with general formula $(Cat)_2[ReX_6]$ and $[Re^{IV}Cl_4(\mu\text{-}ox)Cu^{II}]$ (Tables S3 and S5), geometric parameters of H_2tppz^{2+} (Table S4) and X-ray crystallographic files [CIFS for **1** and **2**].]. See DOI: 10.1039/x0xx00000x

between magnetic centers. So, magneto-structural studies on compounds $(Cat)_m[ReX_6]$ have revealed the occurrence of intermolecular antiferromagnetic interactions between the paramagnetic Re(IV) ions, the exchange pathway being unambiguously provided through space Re–X•••X–Re contacts and the magnetic coupling depending on the spin densities lying on the X ligands as well as on the halogen•••halogen separation between adjacent $[ReX_6]^{2-}$ units in the crystal lattice.[7-9,19,46-50] The last parameter is strongly dependent on the size of the countercation and in this respect, the use of bulky organic cations such as $AsPh_4^+$ and NBu_4^+ can preclude the magnetic coupling between adjacent hexahalorhenate(IV) anions due to the great X•••X separation generated.[8,19] Remarkable magnetic features concern the compounds $K_2[ReI_6]$[8] and $(H_4biim)[ReCl_6]\cdot 4H_2O$.[14] The former one behaves as a weak ferromagnet below 24 K, exhibiting an hysteresis loop at 15 K with a coercive field of 5000 G, whereas a significant ferromagnetic interaction mediated by the long Re–X•••(H_2O)•••X–Re pathway occurs in the latter one.

Focusing on the $[ReCl_4(ox)]^{2-}$ anion which was isolated as $(AsPh_4)_2[ReCl_4(ox)]$ and $(NBu_4)_2[ReCl_4(ox)]$ in 1999 by Chiozzone et al.,[19] it has been proved to be a very suitable precursor for generating anisotropic heterometallic magnetic systems incorporating the Re(IV) ion. The large degree of spin delocalization on the X ligands which is characteristic of the Re(IV) complexes as shown by polarized neutron diffraction experiments and DFT type calculations,[19,35,51,52] is responsible for the strengthening of the magnetic interactions in comparison with analogous systems containing 3d metal ions.[21,24,25,28,30,53] To date, a good number of heterometallic $[Re^{IV}(\mu\text{-ox})M^{II}]$ systems have been characterized, including $[ReCl_4(\mu\text{-ox})Cu(L)_2]$ (L = *bipy*, *phen*, *pyim*),[19,20,27] $[ReCl_4(\mu\text{-ox})Cu(terpy)]\cdot CH_3CN$,[20] $[ReCl_4(\mu\text{-ox})Cu(terpy)(H_2O)][ReCl_4(\mu\text{-ox})Cu(terpy)(CH_3CN)]$,[20] $[CuL_\beta][ReCl_4(\mu\text{-ox})]\cdot DMF$,[22] $(NBu_4)_2[\{ReCl_4(\mu\text{-ox})\}_2M(Him)_2]$ (M = Mn, Ni, Cu, Co),[25] $[ReCl_4(\mu\text{-ox})CuL_\beta]$,[26] $(NBu_4)_4[\{ReCl_4(\mu\text{-ox})\}_3M]$ (M = Fe, Ni, Co, Cu. Mn),[28] $\{(CuL_\alpha)[ReCl_4(ox)]\}_n$,[34] $[ReCl_4(\mu\text{-ox})M(dmphen)_2]\cdot CH_3CN$ (M = Fe, Ni, Mn, Co),[21] $(PPh_4)_2[ReCl_4(\mu\text{-ox})MoO_2Cl_2]$.[54] These studies have shown that the magnetic coupling through the oxalato bridge is ferromagnetic for $\{M^{II}–Re^{IV}\}$ pairs (M = Fe^{II}, Co^{II}, and Ni^{II}) and antiferromagnetic $\{Mn^{II}–Re^{IV}\}$ whereas both types of magnetic interactions are found for $Cu^{II}–Re^{IV}$. Remarkably, the nickel(II) derivative $(NBu_4)_4[\{ReCl_4(\mu\text{-ox})\}_3Ni]$ constitutes the first example of an oxalato-bridged heterometallic species that shows single-molecule magnet (SMM) behavior.[24,28]

In this work we present the synthesis and magneto-structural characterization of two new Re(IV) compounds of formula $H_2tppz[ReCl_6]$ (**1**) (a mononuclear species) and $[Cu(bpzm)_2(\mu\text{-Cl})ReCl_3(\mu\text{-ox})Cu(bpzm)_2(\mu\text{-ox})ReCl_3(\mu\text{-Cl})]_n$ (alternating chain compound) with *tppz* = 2,3,5,6-tetrakis(2-pyridyl)pyrazine and *bpzm* = bis(pyrazol-1-yl)methane.

RESULTS AND DISCUSSION

Synthesis and Characterization.

Compound **1** was prepared by reacting of $K_2[ReCl_6]$ with *tppz* in acidified water-acetonitrile solution whereas **2** was isolated as a highly insoluble polycrystalline powder in the reaction of $(NBu_4)_2[ReCl_4(ox)]$ with the preformed $[Cu(bpzm)_2]^{2+}$ species [generated *in situ* by mixing stoichiometric amounts of copper(II) trifluoromethanesulphonate and *bpzm* in acetonitrile]. Single crystals of **1** were grown by recrystallization in acetonitrile of the solid obtained by evaporation of the mother liquor. In the case of **2**, X-ray quality crystals were obtained by slow diffusion technique in an H-shaped tube.

As shown in Figures S1 and S2 (ESI†), the XRPD patterns measured for the powdered samples of **1** and **2** were in good agreement with the XRPD patterns simulated from the respective single-crystal X-ray data using the Mercury 2.4 program,[55] demonstrating that the crystal structure is truly representative of the bulk material.

Absorption peaks in the regions 1710–1660 cm^{-1} and 1360–1270 cm^{-1} of the infrared spectrum of **2** assigned to the asymmetric and symmetric stretching vibration of the oxalate ligand suggest its coordination as a bridging ligand. The characteristic bands of the ν(C=C) and ν(C=N) stretching modes of bis(pyrazol-1-yl)methane of **2** appear in the range 1630-1510 cm^{-1}. Peaks revealing the presence of H_2tppz^{2+} in **1** in the ranges 3570–3400 cm^{-1} [ν(N–H] and 3100–2700 cm^{-1} [aromatic C–H stretching vibrations], 1620–1530 cm^{-1} [ν(C=N) and ν(C=C) stretches], 1480–990 cm^{-1} [ν(C–C) + ν(C–N) vibrations]. All these spectroscopic features have been confirmed by the crystal structures of **1** and **2** (see below).

Structure Description.

$H_2tppz[ReCl_6]$ (1). The crystal structure of **1** consists of octahedral hexachlororhenate(IV) anions and quasi-planar H_2tppz^{2+} cations held together by electrostatic forces (Fig. 1). Additional N—H•••N hydrogen bonds and weaker C—H•••N, C—H•••Cl, π•••π and π•••Cl type interactions involving the pyridyl rings of the H_2tppz^{2+} cations (Fig. 2 and Table S1, ESI†) contribute to the stabilization of the structure.

Each Re(IV) ion is located on a crystallographic inversion center (the special positions *a* of the $P2_1/c$ space group with the multiplicity 2) and it exhibits a slightly distorted octahedral environment with the Re–Cl bond lengths varying in the narrow range 2.3487(9)-2.3634(9) Å and the *cis* Cl–Re–Cl bond angles being very close to the ideal one of 90° [values in the range 88.96(3)-91.04(3)°] (see Table S2, ESI†).. These values correlate well with those reported in the literature for related species incorporating the $[ReCl_6]^{2-}$ unit (Table S3, ESI†).[1-7,9-16,56] The $ReCl_6$ octahedra form layers parallel to the *bc* plane, in which the neighboring $[ReCl_6]^{2-}$ ions along the [010] direction show a different orientation as they are related by the twofold screw axis (2_1) operation. In the layer, the Re(IV) ions are thoroughly isolated from each other, with the shortest [Re(1)•••Re(1c)] intralayer separation equal 8.896 Å [symmetry code: (c) = 2-*x*, -1/2+*y*, 1/2-*z*]. Similarly, the shortest [Cl(2)•••Cl(1c)] distance of 4.649 Å is considerably longer than the van der Waals contacts (3.62 Å). The anionic layers are well separated from each other by the bulky organic cations, the shortest interlayer distance

being equal to the length of the crystallographic *a* axis [that is 9.9017(5) Å].

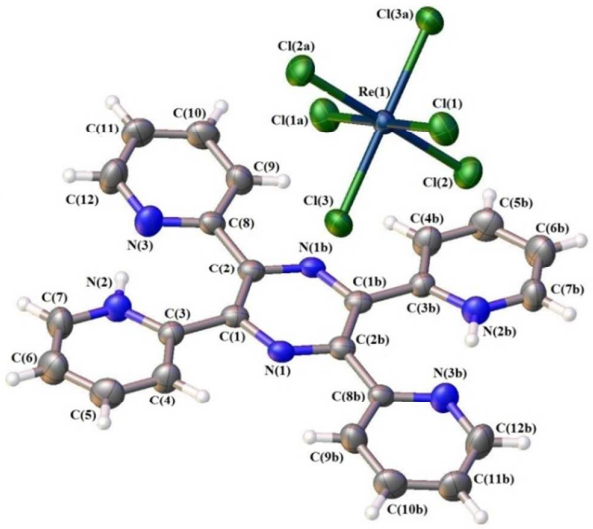

Figure 1. Perspective view of the molecular structure of $H_2tppz[ReCl_6]$ (**1**) showing the atom numbering. Displacement ellipsoids are drawn at the 50% probability level [symmetry code: (a) = 2-*x*, 1-*y*, 1-*z*; (b) = 1-*x*, 1-*y*, 1-*z*].

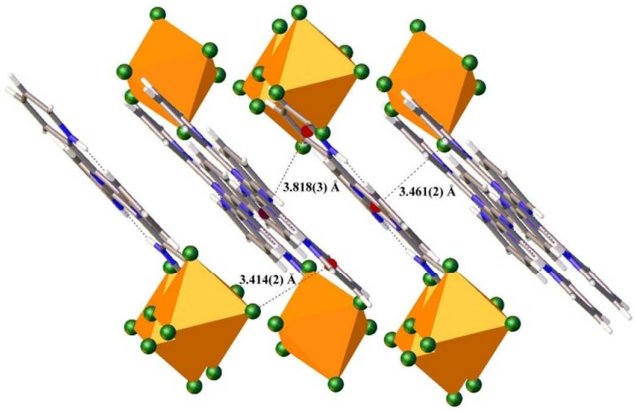

Figure 2. View of the supramolecular packing of **1** arising from hydrogen bonds and weak π•••π and π•••Cl type interactions.

The diprotonated H_2tppz^{2+} cations, situated about an inversion centers lying at the midpoint of the central pyrazine ring, are arranged in layers perpendicular to [101] and they are involved in π•••π stacking contacts [Cg2(N3–C8–C9–C10–C11–C12)•••Cg3^{d}(N2–C3–C4–C5–C6–C7); (d) = *x*, 1/2-*y*, 1/2+*z* with distance 3.818(3) Å] and Re—Cl•••π interactions [Re1–Cl2•••Cg2^{e}(N2–C3–C4–C5–C6–C7); (e) = 1-*x*, 1-*y*, 1-*z* and Re1–Cl3•••Cg1(N1–C1–C2–N1b–C1b–C2b) with distances 3.414(2) Å and 3.461(2) Å, respectively] (Fig. 2).

Due to formation of a short intramolecular hydrogen bond N(2)—H(2)•••N(3) [D•••A distance = 2.549(4)Å and D—H•••A angle = 164.5(2)°] between the two neighbouring pyridine rings (Fig. S3, ESI†), the H_2tppz^{2+} ion in **1** exhibits proton sponge behaviour, likewise in the $(H_2tppz)(I_2•I_3)_2$[57], $(H_2tppz)(Hca)_2$[58], $(H_2tppz)(Hba)_2$[58], $(H_2tppz)(ICl_2)_2$[59], $(H_2tppz)[B(C_6H_5)_4]_2$[60] and $(H_2tppz)[AuCl_4]_2$[61] salts. The structural parameters of the H_2tppz^{2+} ion in these salts were compared in Table S4 (ESI†). The conformation of the cation H_2tppz^{2+} in **1** is related to the "twisted" orientation of the $(H_2tppz)^{2+}$ ion found in the salt $(H_2tppz)(I_2•I_3)_2$[74], but differs from the "bowed" shape of the dication reported for $(H_2tppz)(Hca)_2$[75], $(H_2tppz)(Hba)_2$[75], $(H_2tppz)(ICl_2)_2$[76], $(H_2tppz)[B(C_6H_5)_4]_2$[77] and $(H_2tppz)[AuCl_4]_2$[78] (Fig. S4, ESI†). The major differences involve dihedral angles between the various mean planes of the aromatic rings. The bond distances and angles are essentially the same for these forms. Interestingly, the H_2tppz^{2+} ion from **1** is much closer to planarity in comparison with the "twisted" oriented dication in $H_2tppz(I_2·I_3)_2$ (see Table S4 and Fig. S4, ESI†).

$[Cu(bpzm)_2(\mu\text{-}Cl)ReCl_3(\mu\text{-}ox)Cu(bpzm)_2(\mu\text{-}ox)ReCl_3(\mu\text{-}Cl)]_n$ (2).

The compound **2** crystallizes in the triclinic *P*(-1) space group with the asymmetric unit composed of two halves of $[Cu(bpzm)_2]^{2+}$ cations and one counterion $[ReCl_4(ox)]^{2-}$ (Fig. 3). The two crystallographically independent copper(II) ions [Cu(1) and Cu(2)] lie on inversion centers (special positions *a* and *g* of *P*(-1) space group).

The crystal structure can be described as being made up by alternating $[Cu(1)(bpzm)_2]^{2+}$ and $[(ox)Cl_3Re(\mu\text{-}Cl)Cu(2)(bpzm)_2(\mu\text{-}Cl)ReCl_3(ox)]^{2-}$ units which are interlinked by oxalate ligands to afford a neutral heterobimetallic polymeric chains propagated along the [011] direction (Fig. 4). The oxalate group adopts the didentate (at Re)/monodentate (at Cu) mode. The Re(IV) and Cu(II) centers in the trinuclear $[(ox)Cl_3Re(\mu\text{-}Cl)Cu(2)(bpzm)_2(\mu\text{-}Cl)ReCl_3(ox)]^{2-}$ entities are bridged by single chloro bridges.

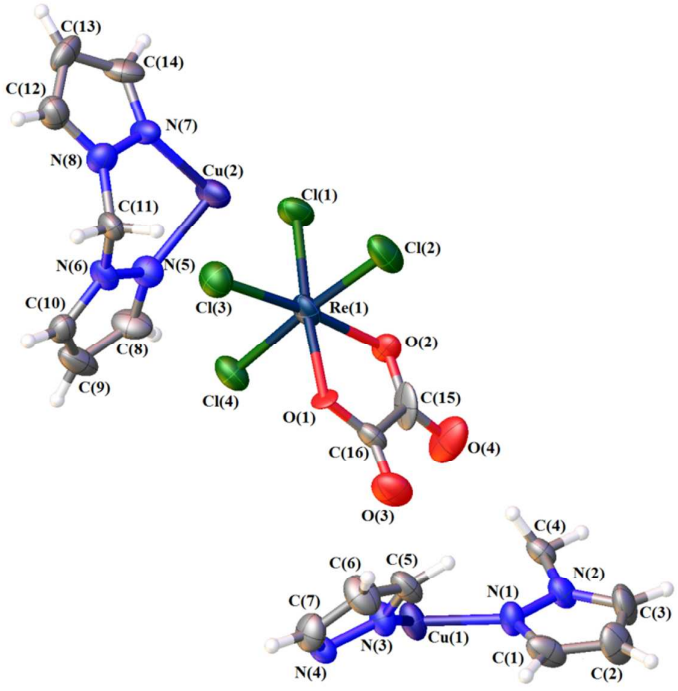

Figure 3. Perspective view of the asymmetric unit of **2** together with atom numbering. Displacement ellipsoids are drawn at the 50% probability level.

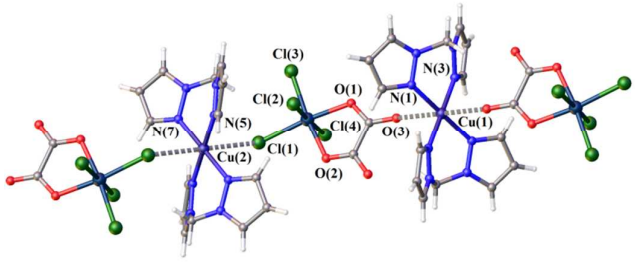

Figure 4. Perspective view of a fragment of the heterobimetallic chain of **2** running parallel to the [011] direction. Weak axial Cu–O and Cu–Cl interactions are shown by broken lines.

The neutral heterobimetallic chains are stabilized additionally by Re—Cl•••π interactions [Re(1)–Cl(2)•••Cg1(N5–N6–C10–C9–C8) with a value of 3.489(7) Å for the chloro atom to centroid distance] (Fig. 5). The value of the shortest interchain chloride-chloride distance is 4.084(4)Å [Cl(2)•••Cl(4f); symmetry code: (f) = 1+x, y, z].

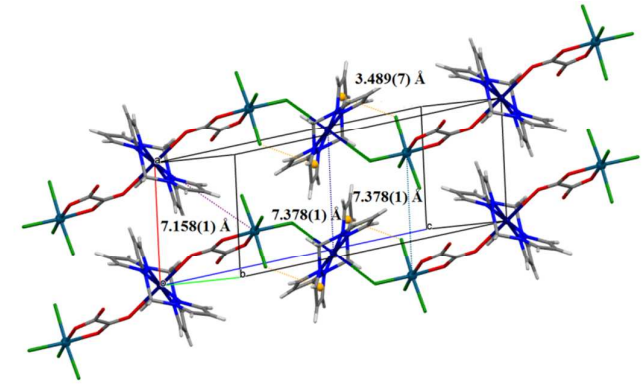

Figure 5. View of the molecular packing of **2** with marked interchain metal-metal distances and intrachain Re—Cl•••π interactions.

The [Re(1)•••Cu(1)] and [Re(1)•••Cu(2)] separations across the didentate–monodentate oxalate and single chloride bridges are 6.478(10) and 4.898(4) Å, respectively. The values of the angles at the oxalate O(3) and chloro Cl(1) atoms of the C(16)–(O(3)–Cu(2) and Re(1)–Cl(1)–Cu(2) pathways are 152.4(10) and 129.0(1)°. The values of the shortest interchain metal-metal distances are 7.378(1) Å [Re(1)•••Re(1f)], 7.378(1) Å [Cu(2)•••Cu(2f)] and 7.158(1) Å [Re(1)•••Cu(1g)] [symmetry code: (f) = = x-1, y, z; (g) = 1-x, 2-y, 2-z] (Fig. 5). A comparison of $[Cu(bpzm)_2(\mu\text{-}Cl)ReCl_3(\mu\text{-}ox)Cu(bpzm)_2(\mu\text{-}ox)ReCl_3(\mu\text{-}Cl)]_n$ motif with the related heterometallic $[Re^{IV}(\mu\text{-}ox)Cu^{II}]$ structures (Table S5, ESI†) shows that the presence of bpzm in the coordination sphere of Cu(II) causes a significantly greater Re•••Cu separation across the oxalate bridge, whereas the separation through the single chloro bridge is comparable with those reported previously.[19,20,22,23,26,27,34.]

The environment of the Cu(1) atom is well described as a tetragonally elongated octahedron with four short bonds formed by the nitrogen atoms from two crystallographically related *bpzm* molecules [2.014(9) and 1.993(10) Å for Cu(1)–N(1) and Cu(1)–N(3), respectively] in the equatorial plane and two oxygen atoms from oxalate ions of adjacent $[ReCl_4(ox)]$ units in axial positions [2.599(11) Å for Cu(1)–O(3) and the symmetry-related Cu(1)–O(3h)] (Table 1).

Table 1. The experimental bond lengths [Å] and angles [°] for **2***

Bond lengths		Bond angles	
Re(1)–O(1)	2.037(8)	O(1)–Re(1)–O(2)	80.5(3)
Re(1)–O(2)	2.065(9)	O(1)–Re(1)–Cl(3)	93.1(2)
Re(1)–Cl(1)	2.348(3)	O(2)–Re(1)–Cl(3)	173.4(2)
Re(1)–Cl(2)	2.356(3)	O(1)–Re(1)–Cl(4)	89.8(2)
Re(1)–Cl(3)	2.323(4)	O(2)–Re(1)–Cl(4)	89.9(3)
Re(1)–Cl(4)	2.326(4)	Cl(3)–Re(1)–Cl(4)	91.47(15)
Cu(1)–N(1)	2.014(9)	O(1)–Re(1)–Cl(1)	172.7(2)
Cu(1)–N(3)	1.993(10)	O(2)–Re(1)–Cl(1)	92.3(2)
Cu(2)–N(5)	2.001(11)	Cl(3)–Re(1)–Cl(1)	94.13(13)
Cu(2)–N(7)	2.024(11)	Cl(4)–Re(1)–Cl(1)	91.17(13)
Cu(1)–O(3)	2.599(11)	O(1)–Re(1)–Cl(2)	86.8(2)
Cu(2)–Cl(2)	3.068(4)	O(2)–Re(1)–Cl(2)	87.3(3)
		Cl(3)–Re(1)–Cl(2)	91.00(13)
		Cl(4)–Re(1)–Cl(2)	175.84(15)
		Cl(1)–Re(1)–Cl(2)	91.99(13)
		N(3)–Cu(1)–N(1)	90.6(4)
		N(3h)–Cu(1)–N(1)	89.4(4)
		N(3h)–Cu(1)–N(1h)	90.6(4)
		N(5)–Cu(2)–N(7)	89.2(4)
		N(5i)–Cu(2)–N(7)	90.8(4)
		N(5i)–Cu(2)–N(7i)	89.2(4)
		Re(1)–Cl(1)–Cu(2)	129.0(1)
		C(16)–O(3)–Cu(1)	152.37(8)

*Symmetry transformations used to generate equivalent atoms: (h) = 2-x, 2-y, 2-z; (i) = 2-x, 1-y, 1-z.

As expected for Cu(II) complexes distorted by Jahn-Teller effect, a significant elongation of the axial Cu–O bond length is observed (see Table 1). Each Re(IV) ion is six-coordinate in a distorted octahedral geometry which is built by four chloride anions and two oxalate-oxygen atoms. The major angular distortion from idealized octahedral geometry is due to the constraints imposed by the didentate oxalate, the angle subtended by this ligand at the rhenium atom being only 80.5(3)° [O(1)–Re(1)–O(2)]. The oxalate group is approximately planar with deviations up to 0.0540(71) Å from the least-squares plane and it makes a dihedral angle of 3.86(52)° with the equatorial plane of Re(1) center formed by the Cl(1)Cl(3)O(1)O(2) set of atoms. The Re–Cl (average value 2.338 Å) and Re–O (average value 2.049 Å) bond lengths are consistent with those reported for related heterobimetallic Cu(II)/Re(IV) complexes.[19,20,22,23,26,27,34]

The Cl(1) ligand of $[ReCl_4(ox)]^{2-}$ is weakly bonded to the copper atom of the centrosymmetric $[Cu(2)(bpzm)_2]^{2+}$ fragment, the Cu(2)–Cl(1) distance being 3.068(4) Å. Taking this very weak interaction into account, the environment of the Cu(2) atom may be described as distorted elongated octahedral (4+2) with two chloro atoms in the axial positions and four nitrogen atoms from two crystallographically related *bpzm*

molecules in the equatorial plane [2.001(11) and 2.024(11) Å for Cu(2)–N(5) and Cu(2)–N(7), respectively].

Each bis(pyrazol-1-yl)methane molecule adopts the didentate coordination mode subtending six-membered chelate rings at the Cu(1) and Cu(2) atoms. These rings exhibit a *boat* conformation with the metal and carbon atoms out the mean plane defined by the four nitrogen atoms. Deviations of Cu(1), Cu(2), C(4) and C(11) atoms from these mean planes are 0.574(3) 0.604(2), 0.665(5) and 0.634(2) Å, respectively.

Magnetic Properties of 1 and 2.

The magnetic properties of **1** in the form of $\chi_M T$ versus T plot [χ_M is the magnetic susceptibility per one Re(IV) ion] are shown in Figure 6. $\chi_M T$ at roomtemperature is 1.61 $cm^3 \cdot mol^{-1} \cdot K$, a value which is as expected for a magnetically isolated Re(IV)ion [the expected $\chi_M T$ value is ca. 1.60 cm^3 mol^{-1} K for S_{Re} = 3/2 and g_{Re} = 1.8-1.9). Upon cooling, $\chi_M T$ remains constant until 100 K and it further decreases to reach 1.02 cm^3 mol^{-1} K at 1.9 K. No maximum of χ_M is observed for **1** in the whole temperature range. The decrease of $\chi_M T$ at low temperatures is due to zero-field splitting effects and/or intermolecular antiferromagnetic interactions. As the crystal packing of **1** shows that the shortest intermolecular chloro•••chloro distances [4.649 Å] are considerable longer than the Van der Waals contacts, the possibility of this magnetic pathway is discarded. The fact that the value of the magnetization for **1** at 2.0 K under the maximum available field in our magnetometer is ca. 1.68 μ_B at 70 kOe (see inset of Figure 6) supports the occurrence of an important zero-field splitting which in the case of Re(IV) (a third row transition metal ion) has its origin in the large value of the spin-orbit coupling parameter (λ ca. 1100 cm^{-1} for the Re(IV) single ion).

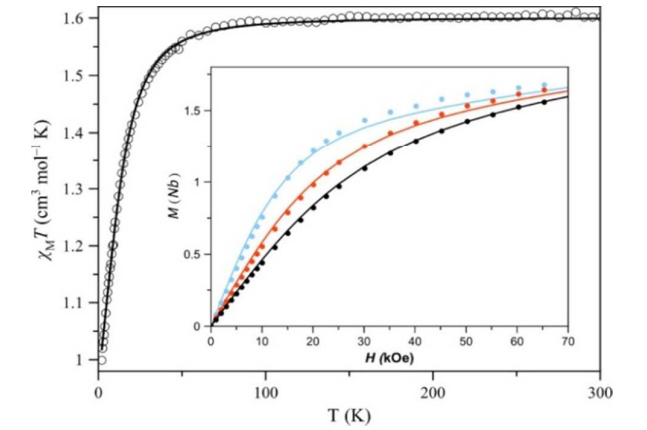

Figure 6. Thermal dependence of $\chi_M T$ (o) for 1. The inset shows the field dependence of the magnetization at 2.0, 3.0 and 4.0 K for the blue, red and black filled circles. The solid lines are the best-fit curves through the spin Hamiltonian of eq (1) (see text).

Having these consideration in mind, we have analyzed the magnetic data of **1** through the spin Hamiltonian of eq (1)

$$\hat{H} = D_{Re}(\hat{S}^2_{zRe} - 5/4) + g^{||}_{Re}\beta H_z \hat{S}^2_{zRe} + g^{\perp}_{Re}\beta(H_x \hat{S}^x_{Re} + H_y \hat{S}^y_{Re}) \quad (1)$$

where $2D_{Re}$ is the energy gap between the M_S =± 3/2 and M_S =± 1/2 (Kramers doublets) and the last two terms account for the Zeeman effect of the anisotropic rhenium(IV) ion. Least-squares best-fit parameters resulting through the simultaneous analysis of the magnetic susceptibility and magnetization data by means of the XVPMAG programme[62] are: D_{Re} = -15.8(2) cm^{-1} and g_{avRe} =1.85(1). The calculated curves reproduce quite well the experimental data. Both the g_{avRe} and D_{Re} values are similar to those obtained for other hexahalorhenate(IV) complexes.[9,11,16,19]

The magnetic properties of **2** in the form of $\chi_M T$ against T plot [$\chi_M T$ is the magnetic susceptibility per $Re^{IV}_2Cu^{II}_2$ unit] are shown in Figure 7. $\chi_M T$ at 295 K is equal to 4.05 cm^3 mol^{-1} K, a value which is as expected for a set of two Re(IV) and two Cu(II) ions magnetically noninteracting ($\chi_M T \approx$ 4.03 cm^3 mol^{-1} K for S_{Re} = 3/2, S_{Cu} = 1/2, gRe = 1.8-1.9 and g_{Cu} = 2.1). Upon cooling, the value of $\chi_M T$ remains constant until 110 K and it further decreases to attain 1.0 $cm^3 \cdot mol^{-1}$ K at 1.9 K. A field-dependent maximum of χ_M is observed which disappears at applied dc magnetic fields $H \geq$ 20 kOe (see bottom inset of Figure 7).

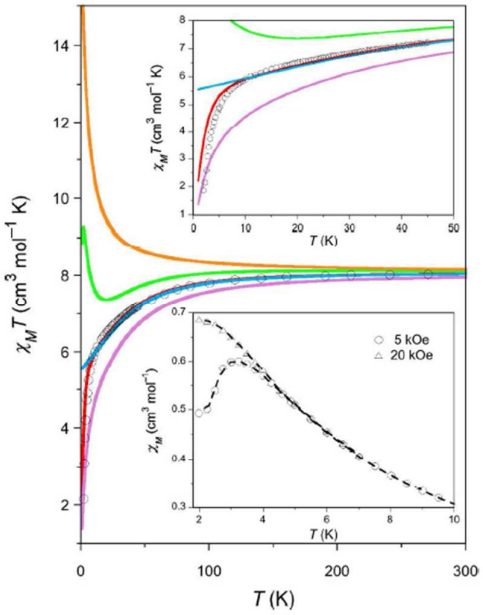

Figure 7. Thermal dependence of $\chi_M T$ (o) for **2**: (o) experimental; (red, blue, magenta and green lines) are the simulated curves through the Hamiltonian of eqns (2a-d) (see text). A detail of the low temperature region is shown in the top inset. The temperature dependence of *M/H* under applied dc fields of 5 (o) and 20 kOe (Δ) is depicted in the bottom inset.

In the light of these features several points deserve to be outlined. Firstly, the Curie law from room temperature to 110 K together with the decrease of $\chi_M T$ below this temperature are not as expected for the occurrence of absolute values of zero-field splitting of the $[ReCl_4(ox)]^{2-}$ unit in the range 50-60 cm^{-1} [a value of D_{Re} equal to -53 cm^{-1} for the Re(IV) in this entity was estimated by HFEPR].[19,22,33,63]

Secondly, the value of $\chi_M T$ at 1.9 K (1.0 $cm^3 \cdot mol^{-1} \cdot K$) is well below that calculated for a set of two Cu(II) and two Re(IV) ions

magnetically isolated, that is with $\chi_M T$ = 2 x 0.41 + 2 x 1.0 = 2.82 cm^3 mol^{-1} K.

In this respect, one has to take into account that the six-coordinate Re(IV) ion at very low temperatures can be regarded as an Ising-type system with a magnetic moment of 2.8 μ_B ($\chi_{av}T$= 1.0 cm^3 mol^{-1} K).[19] The small value of $\chi_M T$ for **2** at 1.9 K is indicative of the occurrence of antiferromagnetic interactions, a feature which is supported by the presence of a maximum of χ_M at 3.0 K. This maximum is observed only at low applied dc fields and it disappears for magnetic fields $H \geq 20$ kOe (metamagnetic-like behaviour). The value of the critical field (H_c = 20 kOe) can be also observed in the magnetization isotherms as the crossing point (Figure 8) and it is indicative of the occurrence of antiferromagnetic interactions.

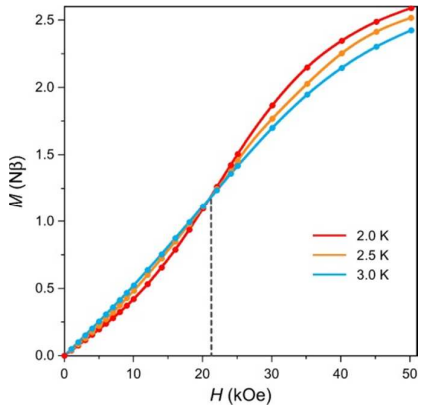

Figure 8. Magnetization isotherms for **2** at the temperatures indicated. The crossing point corresponds to the value of the critical dc magnetic field (Hc).

These anti-ferromagnetic couplings cannot be of intrachain nature because in such a case, they would not lead to a non-magnetic ground spin state. Then, interchain antiferromagnetic interactions are unambiguously present in **2**. Finally, an deep analysis of the magnetic behavior of **2** involves the consideration of the zero-field splitting of the Re(IV) and both the intra- (exchange pathways provided by the didentate/monodentate oxalate and single chloro bridges) and interchain magnetic interactions.

Having in mind the above features and aiming at establishing the best model to analyze the magnetic data of **2**, we have undertaken theoretical studies (CAS and DFT type calculations) to evaluate the relative weight of D_{Re} and those of the intra- and interchain exchange pathways. The two possible intrachain exchange pathways are depicted in Figure 9a [between Re(1) and Cu(1) across the didentate/monodentate oxalate (J_1) and between Re(1) and Cu(2) through the single chloro bridge (J_2)] and Figure 9b [between Re(1) and Cu(1g) across O•••O and C–H•••O (J_3) type interactions and between Re(1) and Re(1f) through Cl•••Cl contacts (J_4)]. In spite of the large delocalization of the spin density of the Re(IV) on its ligands by covalency effects, the fact that the two bridges connect an axial position at the copper(II) ion (the unpaired electron of this ion being mainly delocalized in the equatorial plane) with an equatorial site at the rhenium(IV) center, allows to predict weak intrachain magnetic couplings. This prediction is confirmed by the obtained values for J_1 (+0.21 cm^{-1}) and J_2 (+1.96 cm^{-1}) through DFT type calculations on the respective structural fragments. As far as the two possible interchain magnetic interactions are concerned (Figure 9b), the calculated values are J_3 = -0.007 cm^{-1} and J_4 = -0.06 cm^{-1}.

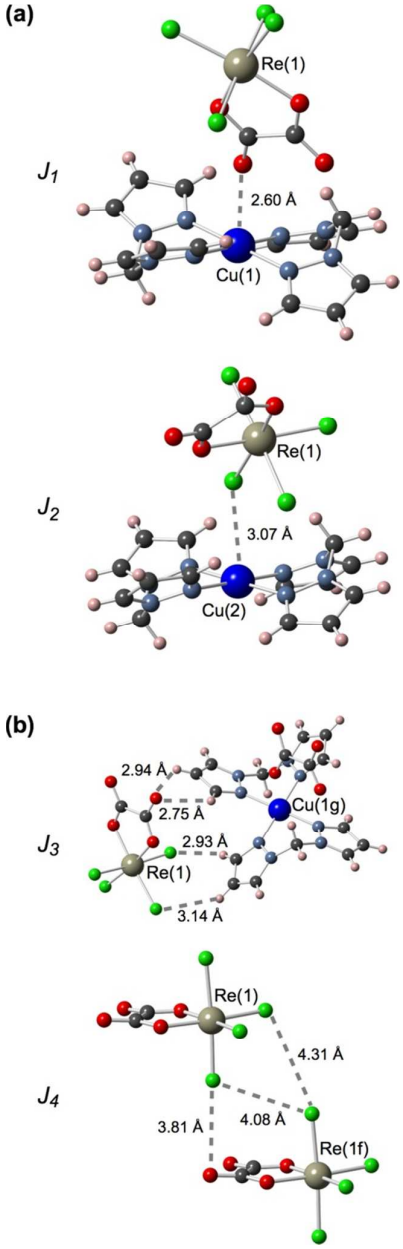

Figure 9. Fragments of the chain structure of **2** showing the possible (a) intra- (J_1 and J_2) and (b) interchain (J_3 and J_4) exchange pathways. The values of the quoted intra- and interchain distances are given in Å.

These results indicate that the two intrachain Re(IV)-Cu(II) magnetic interactions are weak and ferromagnetic, the one through the single chloro bridge being nearly one order of magnitude than that across the oxalate. The greater

delocalization of spin density from the Re(IV) on the chloro ligands compared to that on the O(3) and O(4) oxalate-oxygen atoms in the $[ReCl_4(ox)]^{2-}$ fragment (see Figure 10a), is at the origin of the stronger magnetic coupling through the single chloro bridge. Dealing with the interchain antiferromagnetic interactions, the weak interchain chloro•••chloro contacts involved and the fact that the spin density on the copper(II) unit is located in the equatorial plane (Figure 10b) allows to understand the very weak magnetic couplings for the fragments shown in Figures 9b (J_3 and J_4). Most likely, J_4 would be responsible for the maximum of χ_M observed at very low temperature for **2** and which is overcome by a critical filed $H_c \geq$ 20 kOe. Finally, the value of the $|D_{Re}|$ obtained by a CAS calculation is 47.0 cm^{-1}, its main contribution coming from the doublet excited state (36.9 cm^{-1}). The magnitude of $|D_{Re}|$ in 2 agrees with those previously reported for the $[ReCl_4(ox)]^{2-}$ fragment. [19,22,33,63]

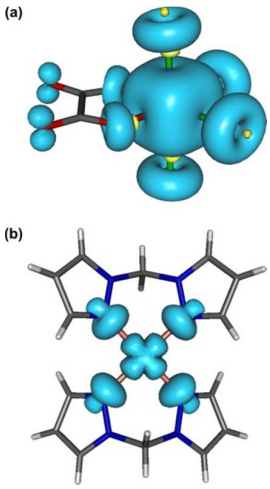

Figure 10. View of the calculated spin density for the S = 3/2 ground spin configuration of the $[ReCl_4(ox)]^{2-}$ anion (a) and the $[Cu(bpzm)_2]^{2+}$ cation (b) in **2**. The isodensity surface corresponds to a cut-off value of 0.002 e $bohr^{-3}$. Blue and yellow isosurfaces correspond to positive and negative regions of spin density, respectively.

In summary, the theoretical calculations on **2** support the occurrence of anisotropic chains with two intrachain ferromagnetic interactions, J_2 [magnetic coupling across the single chloro bridge within the trinuclear Re^{IV}-(μ-Cl)-Cu^{II}-(μ-Cl)-Re^{IV} fragment] and J_1 [magnetic coupling between the Re(IV) and Cu(II) ions from adjacent trinuclear units through the bidentate monodentate oxalate bridge], plus interchain antiferromagnetic interactions through weak Cl•••Cl contacts (J_4).

In the light of the results found above through theoretical calculations, it is clear that the model to be used to simulate the magnetic properties of **2** is quite complicate because of the need for a considerable number of variable parameters. In fact, the magnetic behavior of **2** would correspond to that of an alternating chain where ferromagnetically coupled $(ox)Cl_3Re^{IV}$-(μ-Cl)-$Cu^{II}(bpzm)_2$-(μ-Cl)$Re^{IV}Cl_3(ox)$ trinuclear units (J_2) are linked to $Cu^{II}(bpzm)_2$ mononuclear fragments through the didentate/monodentate oxalate bridge, the magnetic coupling (J_1) being smaller but also of ferromagnetic nature. Moreover, the weak antiferromagnetic interchain magnetic interaction (θ), supported by the field dependent maximum of χ_M at low temperature and which was glimpsed from DFT calculations, has to be taken into account.

Finally, the high anisotropic character of the Re(IV) in the $[ReCl_4(ox)]^{2-}$ fragment is another relevant parameter together with the different average Landé factors of the interacting metal ions (g_{Cu} and g_{Re}). Since the J_1 value is small enough compared to J_2, the magnetic susceptibility data of **2** could be approached through a spin model of eight-sites ring shown in Scheme 1:

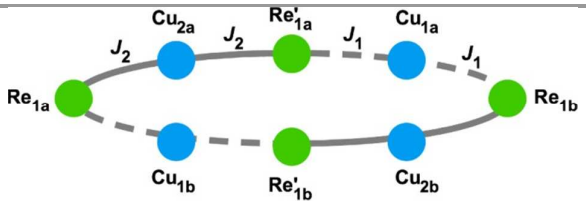

Scheme 1. Ring model for the intrachain exchange couplings in **2**

The spin Hamiltonian for this model with the inclusion of the zfs and Zeeman terms is given by eqns (2a-d):

$$\hat{H} = \hat{H}_{ex} + \hat{H}_{zfs} + \hat{H}_{Zeeman} \quad (2a)$$

$$\hat{H}_{ex} = -J_2[(\hat{S}_{Re1a} + \hat{S}_{Re'1a})\hat{S}_{Cu2a} + (\hat{S}_{Re1b} + \hat{S}_{Re'1b})\hat{S}_{Cu2b}] - J_1[(\hat{S}_{Re'1a} + \hat{S}_{Re1b})\hat{S}_{Cu1a} + (\hat{S}_{Re'1b} + \hat{S}_{Re1a})\hat{S}_{Cu1b}] \quad (2b)$$

$$\hat{H}_{zfs} = \Sigma_i D_{Re_i}(\hat{S}^2_{zRe_i} - 5/4) \quad (2c)$$

$$\hat{H}_{Zeeman} = \beta H \Sigma_i (g_{Re_i}\hat{S}_{Re_i} + g_{Cu_i}\hat{S}_{Cu_i}) \quad (2d)$$

In these equations, the *i* subscript runs over the all rhenium(IV) and copper(II) centers of the ring model. The choice of a smaller size ring would be too risky and a bigger one would involve an excessive cpu-time cost without any significant progress in the simulation of the magnetic data in the temperature range investigated.

The interchain interactions were introduced into the model as a θ term. Among the different values for the J_1, J_2, D_{Re}, g_{Cu}, gRe and θ parameters, we have selected the set of them that having coherent values with the theoretical ones, best reproduce the experimental magnetic data. A good simulation of the magnetic data (red curve in Figure 7) was obtained with the following set of parameters: J_1 = +0.15 cm^{-1}, J_2 = +4.9 cm^{-1}, $|D_{Re}|$ = 42 cm^{-1},g_{Re} = 1.85, g_{Cu} = 2.10 and θ = -3.0 K. Concerning these values, it deserves to be noted that J_2 and J_1 play an opposite role to those of D_{Re} and θ. In our simulations, by decreasing the value of J_2 to approach that obtained through DFT, the magnitudes of D_{Re} and θ also decrease but the experimental data are poorer reproduced. Because of the great number of variable parameter parameters (J_1, J_2 , J_3, J_4, D_{Re}, θ, g_{Cu} and g_{Re}), we have fixed the values of the Landé factors to the usual values from the literature. This has reduced the complexity of the system without any significant loss of physical meaning in the simulation. However, we are still faced to a

complex situation. Also, it has to be recalled that the evaluation of the intermolecular magnetic interactions by DFT calculations is uncommon and it requires functionals that include long-range corrections and/or dispersion models.[64] Anyway, the intermolecular distances can change with the temperature and consequently, the size of the intermolecular magnetic interactions would be modified.

In order to get a better understanding of the influence and need for each of the involved parameters for **2**, we have performed different simulations in which the above values of the parameters were used, some of them being systematically removed. So, when considering D_{Re}, g_{Cu} and g_{Re} as the only parameters (blue line in Fig. 7), the experimental data can be properly simulated only at high temperatures whereas the experimental data abruptly fall and they remain well below the limit value for the theoretical one at very low temperatures. Therefore, an antiferromagnetic coupling is needed. Its inclusion as θ in addition to D_{Re}, g_{Re} and g_{Cu} generates a curve (magenta line in Fig. 7) that is close to the experimental data at high and low temperatures but far from those in the intermediate region. On the other hand, when J_2, D_{Re}, g_{Re} and g_{Cu} are considered to calculate the theoretical curve (green line in Fig. 7), one can see how the values of $\chi_M T$ decrease upon cooling from room temperature because of the dominant zfs, but they increase at low temperatures due to the effect of the intrachain ferromagnetic coupling. Then, an antiferromagnetic interchain interaction would be needed to cause the observed $\chi_M T$ decrease at low temperatures. In fact, a quite good match of the experimental magnetic data of 2 is only achieved by considering all the intra- and interchain magnetic interactions plus de zfs and Landé factors (red line in Fig. 7), the good model being inspired by the results obtained through theoretical DFT and CAS calculations.

CONCLUSIONS

The magneto-structural study of a mononuclear Re(IV) complex (**1**) and a heterobimetallic Re(IV)-Cu(II) chain (**2**), the former compound being an ionic salt and the second one a neutral one-dimensional species with alternating single chloro and didentate/monodentate oxalato bridges, has shown the importance of the accurate structural knowledge and theoretical calculations aiming at interpreting and simulating the magnetic properties of systems where the magnetic anisotropy is a leading term together with the occurrence of magnetic interactions. **1** behaves as a magnetically isolated Re(IV) compound whose magnetic behavior is dictated by the relatively high anisotropy of the hexachlororhenate(IV). The magnetic isolation of the Re(IV) centers in **1** is ensured by the bulky diprotonated H_2tppz^{2+} organic cation. The occurrence of a large zfs of the Re(IV), intrachain ferro- and antiferromagnetic couplings together with interchain magnetic interactions, these last ones being responsible for the observed metamagnetism, make very difficult the interpretation of the magnetic data of **2**. In such a case the choice of the best model to simulate the magnetic data in the whole temperature range investigated was obtained by evaluating the relative magnitude and nature of the involved parameters by DFT and CAS calculations on the corresponding fragments of the real structure.

EXPERIMENTAL SECTION

Materials and methods.

Bis(pyrazol-1-yl)methane and $(NBu_4)_2[ReCl_4(ox)]$ were prepared as previously reported.[19,65,66] The other reagents used in the synthesis were commercially available (POCH and Aldrich) and they were used without further purification. IR spectra were recorded on a Nicolet iS5 spectrophotometer in the spectral range 4000-400cm^{-1} with the samples as KBr pellets. X-ray powder diffraction (XRPD) measurements [Figs. S1 (**1**) and S2 (**2**), ESI†] were performed on a PANalytical Empyrean X-ray diffractometer using Cu−Kα radiation (λ = 1.5418 Å), in which the X-ray tube was operated at 40 kV and 30 mA ranging from 5 to 50°. Variable-temperature (1.9-300 K) direct current (dc) magnetic susceptibility measurements under applied magnetic fields of 10 kOe (50 ≤ T ≤ 300 K) and 250Oe (T < 50 K) and field-dependence (0-70 kOe) magnetization measurements at low temperatures were carried out with a Quantum Design SQUID magnetometer. The magnetic data were corrected for the diamagnetic contribution of the constituent atoms and the sample holder.

Preparation of $H_2tppz[ReCl_6]$ (1).

$K_2[ReCl_6]$ (0.50 g, 1.0 mmol) dissolved in 10 mL of 1 M HCl was added to the acetonitrile solution (50 mL) of tppz (0.38 g, 1 mmol) and the resulting solution was refluxed for 4 h under continuous stirring. It was then allowed to evaporate until reaching a small volume (10 mL) and cooled at room temperature. The red crystalline solid of **1** which separated was filtered off and dried in the open air. X-ray quality brown polyhedra of **1** were obtained by slow recrystallization from acetonitrile and collected by filtration. Yield: 631 mg (80%). Anal. Calc. for $C_{24}H_{18}Cl_6N_6Re$ (1): C, 36.52; H, 2.30; N, 10.65. Found: C, 36.68; H, 2.42; N, 10.84%. IR (KBr/cm^{-1}): 3561(w) and 3417(w) [ν(N–H)]; 1611(s) and 1543(m) [$\nu(C{=}N_{tppz})$] and [$\nu(C{=}C_{tppz})$].

Preparation of $[Cu(bpzm)_2(\mu\text{-}Cl)ReCl_3(\mu\text{-}ox)Cu(bpzm)_2(\mu\text{-}ox)ReCl_3(\mu\text{-}Cl)]_n$ (2).

$(NBu_4)_2[ReCl_4(ox)]$ (0.1 g, 0.11 mmol) dissolved in water (5 mL) was slowly added to an acetonitrile solution (5 mL) containing copper(II) trifluoromethanesulfonate (0.40 g, 0.11 mmol) and bpzm (0.32 g, 0.22 mmol). A blue crystalline solid appeared in some minutes, and the crystallization was complete after 24 h. Yield: 430 mg (70%). X-ray quality crystals of **2** as blue plates were grown by slow diffusion in an H-shaped tube. Copper(II) trifluoromethanesulfonate (0.055 mmol) and bis(pyrazol-1-yl)methane (0.11 mmol) dissolved in acetonitrile were placed at the bottom of one arm, and a concentrated acetonitrile solution of $(NBu_4)_2[ReCl_4(ox)]$ (0.11 mmol) was introduced into the other arm. Then, acetonitrile was carefully added to both arms to fill the H-tube, covered with parafilm and the whole was allowed to diffuse at room temperature. Blue crystals of **2**

were grown after one week. Yield: 307 mg (50%). *Anal.* Calc. for $C_{32}H_{32}Cl_8Cu_2N_{16}O_8Re_2$ (**2**): C, 24.77; H, 2.08; N, 14.44. Found: C, 24.66; H, 2.14; N, 14.65%. IR (KBr/cm^{-1}): 1706(vs) and 1676 (m) [ν_{as}(COO)]; 1602(w) and 1513(w) [ν(C=N$_{bpzm}$)] and [ν(C=C$_{bpzm}$)]; 1357(s) and 1286(s) [ν_s(COO)].

Crystal Structure Determination and Refinement.

The X-ray diffraction data on single crystals of **1** and **2** were collected on an Oxford Diffraction four-circle diffractometer Gemini A Ultra with Atlas CCD detector by using graphite-monochromated MoKα radiation (λ = 0.71073 Å) at room temperature. A summary of the crystal data and refinement details of the structures of **1** and **2** is given in Table 2. Lorentz, polarization and empirical absorption correction using spherical harmonics implemented in SCALE3 ABSPACK scaling algorithm[67] were applied. The structures were solved by the direct methods and refined by full-matrix least-squares on F^2 using SHELXL97.[68] All the non-hydrogen atoms were refined anisotropically using full-matrix least-squares technique. Hydrogen atoms bound to carbon atoms were placed in calculated positions and treated as riding on their parent atoms with d(C–H) = 0.93 A, U_{iso}(H) = 1.2 U_{eq}(C) (aromatic). Selected bond lengths and angles are listed in Tables 1 (**1**) and 2 (**2**) whereas the hydrogen bonds and C–H•••O, C–H•••Cl and C–H•••N type interactions are grouped in Table S1 (**1** and **2**).

Table 2. Crystal data and structure refinement for complexes **1** and **2.**

	1	**2**
Empirical formula	$C_{24}H_{18}Cl_6N_6Re$	$C_{32}H_{32}Cl_8Cu_2N_{16}O_8$
Formula weight [g mol^{-1}]	789.34	1551.82
Temperature [K]	293(2)	293(2)
Wavelength [Å]	0.71073	0.71073
Crystal system	Monoclinic	Triclinic
Space group	$P2_1/c$	P-1
Unit cell dimensions [Å, deg]	a = 9.9017(5)	a = 7.3780(6)
	b = 14.8558(5)	b = 8.9895(5)
	c = 9.7532(4)	c = 18.1306(8)
		α = 86.077(4)
	β= 111.682(6)	β = 85.878(5)
		γ = 80.447(6)
Volume [Å^3]	1333.17(10)	1180.81(13)
Z	2	1
Density (calculated) [Mg m^{-3}]	1.966	2.182
Absorption coefficient [mm^{-1}]	5.187	6.516
F(000)	762	744
Crystal size [mm]	0.027x0.048x0.110	0.123x0.052x0.045
θ range for data collection [°]	3.53 to 25.05	3.31 to 25.05
Index ranges	-9≤h≤11	-8 ≤h≤8
	-17≤k≤17	-10 ≤k≤10
	-11≤l≤11	-21≤ l ≤21
Reflections collected	6356	10532
Independent reflections	2357	4149
	[R_{int} = 0.0338]	[R_{int} = 0.1112]
Completeness to 2θ = 25°	99.8%	99.7%
Min. and max. transm.	0.489 and 1.000	0.663 and 1.000
Data/restraints/parameters	2357 / 0 / 169	4169 / 0 / 310
Goodness-of-fit on F^2	0.971	0.962
Final R indices [I > 2σ(I)]	R_1 = 0.0232	R_1 = 0.0688
	wR_2 = 0.0420	wR_2 = 0.1433
R indices (all data)	R_1 = 0.0363	R_1 = 0.1137
	wR_2 = 0.0446	wR_2 = 0.1576
Largest diff. peak/hole (e Å^{-3})	0.691/-0.528	2.517/-1.717

Crystallographic data for the structures of **1** and **2** have been deposited at the Cambridge Crystallographic Data Centre with the CCDC reference numbers 1062548 (**1**) and 1062549 (**2**). See the Supporting Information for crystallographic data in CIF format.

Computational Details.

All calculations of the zfs parameters were performed with the version 3.0 of the ORCA program system.[69] A TZVP basis set proposed by Ahlrichs and tight SCF criteria were used in all cases.[70,71] Relativistic effects on the electronic effects for the rhenium atom were introduced from zero-order regular approximation (ZORA).[72] For complete active space (CAS) calculations, this auxiliary basis set was replaced by TZV/C.[73-75] Experimental geometries of **1** and **2** were used in the theoretical calculations. The zfs parameters were evaluated from CAS calculations by including contributions from ten quartet and twenty doublet states generated from electron promotion between d orbitals, which corresponds to the full active space built from only the five d orbitals of the Re(IV) ion. From a broken symmetry approach to DFT methodology using the CAM-B3LYP functional as was implemented in Gaussian 09,[76,77] intra- and intermolecular magnetic interactions were calculated. In this case, double-ζ and Los Alamos effective core potentials proposed by Hay and Wadt were used for the Re atom.[78-80] Ahlrichs double- ζ basis set was used for the rest of atoms.[71] The two-electron integrals and their derivatives were commuted in such cases from a Douglas-Kroll-Hess (DKH) 2nd order scalar relativistic calculation.[81] Electronic effects by surrounding molecules in the network were simulated by a polarizable continuum model with the parameters corresponding to the acetonitrile solvent.[82]

ACKNOWLEDGMENTS

This work was supported by the Polish National Science Centre (Grant No. DEC-2012/05/N/ST5/00743 and DEC-2012/07/N/ST5/02213) and the Spanish MICINN (Project CTQ-2013-44844P). Joanna Palion-Gazda is grateful for a scholarship from the DoktoRIS project cofinanced by the European Social Fund.

Notes

The authors declare no competing financial interest.

REFERENCES

1 E. Adman and T. N Margulis, *Inorg. Chem.,* 1967, **6**, 210.
2 E. J. Lisher, N. Cowlam and L. Gillott, *Acta Cryst. Sect. B*, 1979, **35**, 1033.
3 M. Bettinelli, C. D. Flint and G. Ingletto, G. *J. Mater. Chem.,* 1991, **1**, 437.
4 R. Loris, D. Maes, J. Lisgarten, M. Betinelli and C. Flint, *Acta Cryst. Sect. C,* 1993, **49**, 231.
5 L. J. Barbour, L. R. MacGilivray and J. L. Atwood, *J. Chem. Crystal.,* 1996, **26**, 59.

6 C. J. Kepert, M. Kurmoo, and P. Day, *J. Mater. Chem.*, 1997, **7**, 221.
7 J. Mroziński, A. Kochel and T. Lis, *J. Mol. Struct*., 2002, **641**, 109.
8 R. Gonzaléz, R. Chiozzone, C. Kremer, G. De Munno, F. Nicolo, F. Lloret, M. Julve and J. Faus, *Inorg. Chem.,* 2003, **42**, 2512.
9 R. Gonzaléz, R. Chiozzone, C. Kremer, F. Guerra, G. De Munno, F. Lloret, M. Julve and J. Faus, *Inorg. Chem.,* 2004, **43**, 3013.
10 A. Kochel, *Acta Cryst. Sect. E,* 2004, **60**, m859‑m860.
11 R. Gonzaléz, F. Romero, D. Luneau, D. Armentano, G. De Munno, C. Kremer, F. Lloret, M. Julve, and J. Faus, I*norg. Chim. Acta,* 2005, **358**, 3995.
12 M. Hołyńska, M. Korabik, M. and T. Lis, *Acta Cryst. Sect. E,* 2006, **62**, m3178.
13 J. Martinez-Lillo, D. Armentano, G. De Munno, F. Lloret, M. Julve, and J. Faus, *Cryst. Growth Des.,* 2006, **6**, 2204.
14 J. Martinez-Lillo, D. Armentano, G. De Munno, N. Marino, F. Lloret, M. Julve, and J. Faus, *CrystEngComm,* 2008, **10**, 1284.
15 D. Armentano, and J. Martinez-Lillo, *Inorg. Chim. Acta,* 2012 **380**, 118.
16 F. Pop, M. Allain, P. Auban-Senzier, J. Martinez-Lillo, F. Lloret, M. Julve, E. Canadell and N. Avarvari, *Eur. J. Inorg. Chem.,* 2014, 3855.
17 K. S. Pedersen, M. Sigrist, M. A. Sorensen, A.-L. Barra, T. Weyhermuller, S. Piligkos, C. A. Thuesen, M. G. Vinum, H. Mutka, H. Weihe, R. Clerac, and J. Bendix, *Angew. Chem. Int. Ed.,* 2014, **53**, 1351.
18 J. Martinez-Lillo, J. Faus, F. Lloret, and M. Julve, *Coord. Chem. Rev.,* 2015, **289-290**, 215.
19 R. Chiozzone, R. Gonzaléz, C. Kremer, G. De Munno, J. Cano, F. Lloret, M. Julve, and J. Faus, *Inorg. Chem.,* 1999, **38**, 4745.
20 R. Chiozzone, R. Gonzaléz, C. Kremer, G. De Munno, D. Armentano, J. Cano, F. Lloret, M. Julve and J. Faus, *Inorg. Chem.,* 2001, **40**, 4242.
21 R. Chiozzone, R. Gonzaléz, C. Kremer, G. De Munno, D. Armentano, F. Lloret, M. Julve and J. Faus, *Inorg. Chem.* 2003, **42**, 1064.
22 A. Tomkiewicz, J. Mroziński, I. Brüdgam and H. Hartl, *Eur. J. Inorg. Chem.,* 2005, 1787.
23 A. Tomkiewicz, J. Mroziński, B. Korybut-Daszkiewcz, I. Brüdgam and H. Hartl, *Inorg. Chim. Acta*, 2005, **358**, 2135.
24 J. Martinez-Lillo, D. Armentano, G. De Munno, W. Wernsdorfer, M. Julve, F. Lloret and J. Faus, *J. Am. Chem. Soc.,* 2006, **128**, 14218.
25 J. Martinez-Lillo, F. S. Delgado, C. Ruiz-Perez, F. Lloret, M. Julve and J. Faus, *Inorg. Chem*., 2007, **46**, 3523.
26 A. Bieńko, J. Kłak, J. Mroziński, R. Kruszyński, D. C. Bieńko and R. Boća, *Polyhedron,* 2008, **27**, 2464.
27 J. Martinez-Lillo, D. Armentano, G. De Munno, F. Lloret, M. Julve and J. Faus, *Dalton Trans.,* 2008, 40.
28 J. Martinez-Lillo, D. Armentano, G. De Munno, W. Wernsdorfer, J. M. Clemente-Juan, J. Krzystek, F. Lloret, M. Julve and J. Faus, *Inorg. Chem.,* 2009, **48**, 3027.
29 R. Chiozzone, R. Gonzaléz, C. Kremer, D. Armentano, G. De Munno, M. Julve and F. Lloret, *Inorg. Chim. Acta,* 2011, **370**, 394.
30 J. Martinez-Lillo, T. F. Mastropietro, G. De Munno, F. Lloret, M. Julve and J. Faus, *Inorg. Chem.*, 2011, **50**, 5731.
31 J. Martinez-Lillo, L. Cañadillas-Delgado, J. Cano, F. Lloret, M. Julve and J. Faus, *Chem. Commun.,* 2012, **48**, 9242.
32 J. Martinez-Lillo, D. Armentano, G. De Munno, M. Julve, F. Lloret and J. Faus, *Dalton Trans.,* 2013, **42**, 1687.
33 J. Martinez-Lillo, T. F. Mastropietro, E. Lhotel, C. Paulsen, J. Cano, G. De Munno, J. Faus, F. Lloret, M. Julve, S. Nellutla and J. Krzystek, *J. Am. Chem. Soc.,* 2013, **135**, 13737.
34 A. Bieńko, R. Kruszyński and D. Bieńko, *Polyhedron*, 2014, **75**, 1.
35 A. Cuevas, R. Chiozzone, C. Kremer, L. Suescun, A. Mombrú, D. Armentano, G. De Munno, F. Lloret, J. Cano, J. Faus, *Inorg. Chem.,* 2004, **43**, 7823.
36 A. Cuevas, C. Kremer, L. Suescun, S. Russi, A. W. Mombrú, F. Lloret, M. Julve and J. Faus, *Dalton Trans.* 2007, 5305.
37 A. Cuevas, C. Kremer, L. Suescun, S. Russi, A. W. Mombrú, F. Lloret, M. Julve and J. Faus, *Dalton Trans.,* 2010, **39**, 11403.
38 T. D. Harris, M. V. Bennett, R. Clérac, J. R. Long, *J. Am. Chem. Soc.,* 2010, **132**, 3980.
39 T. D. Harris, C. Coulon, R. Clérac and J. R. Long, *J. Am. Chem. Soc*., 2011, **133**, 123.
40 T. D. Harris, H. S. Soo, C. J. Chang and J. R. Long, *Inorg. Chim. Acta,* 2011, **369**, 82.
41 X. Feng, T. D Harris and J. R. Long, *Chem. Sci.,* 2011, **2**, 1688.
42 I. Bhowmick, E. A. Hilard, P. Decahmbenoit, C. Coulon, T. D. Harris and R. Clérac, *Chem. Commun.*, 2012, **48**, 9717.
43 I. Bhowmick, T. D. Harris, P. Dechambenoit, E. A. Hilard, C. Pichon, J. Ie-Rang, and R. Clérac, *Sci. China Chem.,* 2012, **55**, 1004.
44 X. Feng, J. Liu, T. D. Harris, S. Hill and J. R. Long, *J. Am. Chem. Soc.,* 2012, **134**, 7521.
45 Y.-Q. Zhang, C.-L. Luo, X.-B. Wu, B.-W. Wang and S. Gao, *Inorg. Chem.,* 2014, **53**, 3503.
46 R. H. Busey and E. Sonder, *J. Chem. Phys.,* 1962, **36**, 93.
47 H. G. Smith and G. E. Bacon, *J. Appl. Phys.,* 1966, **37**, 979.
48 V. Minkiewicz, G. Shirane, B. Frazer, R. Wheeler and P. Dorain, *J. Phys. Chem. Solids*, 1968, **29**, 881.
49 A. Tomkiewicz, F. Villain and J. Mroziński, *J. Mol. Struct.,* 2000, **555,** 383.
50 J. Martinez-Lillo, J. Kong, M. Julve and E. K. Brechin, *Cryst. Growth Des.,* 2014, **14**, 5985.
51 P. A. Reynolds, B. Moubaraki, K. S. Murray, J. V. Cable, L. M. Engelhardt and B. N. Figgis, *J. Chem. Soc., Dalton Trans.*, 1997, 263.
52 P. A. Reynolds, B. N. Figgis and D. Martin y Marero, *J. Chem. Soc., Dalton Trans.*, 1999, 945.
53 Y. Pei, Y. Journaux and O. Kahn, *Inorg. Chem.,* 1989, **28**, 100.
54 J. Martinez-Lillo, D. Armentano, G. De Munno, F. Lloret, M. Julve, and J. Faus, *Dalton Trans.*, 2011, **40**, 4818.
55 C. F. Macrae, I. J. Bruno, J. A. Chisholm, P. R. Edfinfton, P. McCabe, E. Pidcock, L. Rodriguez-Monge, R. Taylor, J. van de Streek and P. A. Wood, *J. Appl. Crystallogr.*, 2008, **41**, 466.
56 J. Martinez-Lillo, J. Komg, W. P. Barros, J. Faus, M. Julve and E. K. Brechin, *Chem. Commun.,* 2014, **50**, 5840.
57 C. W. Padgett, R. D. Walsh, G. W. Drake, T. W. Hanks, and W. T. Pennington, *Cryst. Growth Des.* 2005, **5**, 745.
58 S. Horiuchi, R. Kumai, Y. Tokunaga and Y. Tokura, *J. Am. Chem. Soc.*, 2008, **130**, 13382.
59 M. C. Aragoni, M. Arca, F. A. Devillanova, M. B. Hursthouse, S. L. Huth, F. Isaia, V. Lippolis, A. Mancini, H. R. Ogilvie and G. Verani, *J. Organomet. Chem*., 2005, **690**, 1923.
60 H. Bock, T. Vaupel, C. Näther, K. Ruppert and Z. Havlas, *Angew. Chem., Int. Ed. Engl.*, 1992, **31**, 299.
61 A. Abedi, A. Dabbaghi and V. Amani, *Acta Crystallogr., Sect. E* 2011, **67**, m1375.
62 J. Cano, *XVPMAG package*, University of Valencia, Spain, 2013.
63 A. Tomkiewicz, T. J. Bartczak, R. Kruszyński and J. Mroziński, *J. Mol. Struct.*, 2001, **595**, 225.
64 J. Martínez-Lillo, J. Cano, W. Wernsdorfer, and E. K. Brechin, *Chem. Eur. J.,* 2015, 21, 8790.
65 S. Julia, P. Sala, J. Del Mazo, M. Sancho, C. Ochoa, J. Elguero, J. P. Fayet and M. C. Vertut, *J. Heterocyclic Chem*., 1982, **19**, 1141‑1145.
66 E. Diez-Barra, A. de la Hoz, A. Sanchez-Migallón and J. Tejeda, *Heterocycles*, 1992, **34**, 1365.
67 *CrysAlis RED*, Oxford Diffraction Ltd., Version 1.171.35.11, 2011

68 G. M. Sheldrick, *Acta Cryst*., 2008, **A64**, 112.
69 F. Neese, WIREs *Computational Molecular Science*, 2012, **2**, 73.
70 A. Schafer, C. Huber and R. J. Ahlrichs, *Chem. Phys.* 1994, **100**, 5829.
71 A. Schafer, H. Horn and R. Ahlrichs, *J. Chem. Phys.* 1992, **97**, 2571.
72 C. Cheng, M. Pelissier and P. Durand, *Phys. Scr.* 1986, **34**, 394.
73 K. Eichkorn, O. Treutler, H. Ohm, M. Haser and R. Ahlrichs, *Chem. Phys. Lett.*, 1995, **240**, 283.
74 K. Eichkorn, O. Treutler, H. Ohm, M. Haser and R. Ahlrichs, *Chem. Phys. Lett.*, 1995, **242**, 652.
75 K. Eichkorn, F. Weigend, O. Treutler and R. Ahlrichs, *Theor. Chem. Acc.*, 1997, **97**, 119.
76 T. Yanai, D. P. Tew and N. C. Handy, *Chem. Phys. Lett.*, 2004, **393**, 51.
77 M. J. Frisch, *et al.*, Gaussian 09, (Rev. D01); Gaussian, Inc., Wallingford, CT, 2009.
78 P. J. Hay and W. R. Wadt, *J. Chem. Phys.*, 1985, **82**, 270.
79 P. J. Hay and W. R. Wadt, *J. Chem. Phys.*, 1985, **82**, 299.
80 W. R. Wadt and P. J. Hay, *J. Chem. Phys.,* 1985, **82**, 284.
81 B. A. Hess, *Phys. Rev. A*, 1985, **32**, 756.
82 J. Tomasi, B. Mennucci and R. Cammi, *Chem. Rev.*, 2005, **105**, 2999.

Table of Contents Graphic and Synopsis

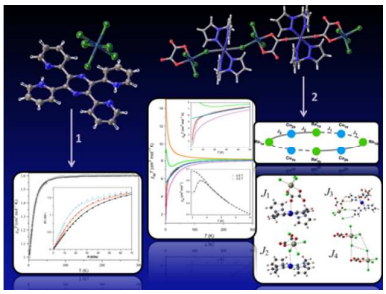

The magneto-structural study of a mononuclear $(H_2tppz)[ReCl_6]$ ionic salt and a heterobimetallic $[Cu(bpzm)_2(\mu\text{-}Cl)ReCl_3(\mu\text{-}ox)Cu(bpzm)_2(\mu\text{-}ox)ReCl_3(\mu\text{-}Cl)]_n$ chain with alternating single chloro and didentate/monodentate oxalato bridges is presented here.